In-situ NMR study of dislocation motion in Ca++-doped NaCl crystals

Michael, K; Kanert, O; Kuchler, R; De Hosson, JTM

Published in:
Solid State Communications

DOI:
10.1016/j.ssc.2003.12.018

Publication date:
2004

Available online at www.sciencedirect.com
SCIENCE DIRECT®
Solid State Communications 129 (2004) 727–731
solid state communications
www.elsevier.com/locate/ssc

In-situ NMR study of dislocation motion in Ca^{++}-doped NaCl crystals

K. Michael[a], O. Kanert[a,*], R. Küchler[a], J.Th.M. De Hosson[b]

[a]*Institute of Physics, University of Dortmund, Otto-Hahn-Str. 4, 44221 Dortmund, Germany*
[b]*Department of Applied Physics, University of Groningen, 9747 AG Groningen, The Netherlands*

Received 4 December 2003; received in revised form 9 December 2003; accepted 10 December 2003 by M. Cardona

Abstract

Using a fast multi-window NMR technique, we have measured in-situ the mean jump width x of mobile dislocations during plastic deformation in a series of NaCl single crystals with varying Ca^{++} content. Aside from immobile forest dislocations, the Ca^{++} impurities form additional obstacles for the moving dislocations thus lowering x. We found that the Ca^{++}-related obstacles exhibit a pronounced non-random distribution which results in a corresponding broad distribution of x. We show that the data can be evaluated by means of an appropriate distribution function $g(1/x)$ with an uncommon dependence of the observed fitting parameters on the Ca^{++} content. As expected, quenching of a sample leads to a more uniform distribution of the Ca^{++}-related obstacles resulting in a corresponding narrowing of $g(1/x)$.

PACS: 61.70.Le; 62.20.Fe; 76.60.Es

Keywords: C. Dislocation motion; E. Nuclear spin relaxation

1. Introduction

The plastic deformation of fcc structured crystalline materials is controlled by a jerky motion of dislocations where immobile lattice defects such as forest dislocations, impurity atoms, or grain boundaries act as obstacles for the moving dislocations. The applied strain rate $\dot{\varepsilon}$ is linked to the mean velocity $\langle v\rangle = x/\tau$ of the mobile dislocations with density ρ_m by the Orowan equation [1]

$$\dot{\varepsilon} = B\cdot\rho_m\cdot x/\tau \tag{1}$$

where B is of the order of the magnitude b of the Burgers vector, x denotes the mean jump width of the mobile dislocations waiting a time τ at an obstacle between two successive jumps.

The dislocation movements cause fluctuating electric field gradients (EFGs) which give rise to a quadrupolar nuclear spin relaxation (NSR) process of suitable probe nuclei with nuclear spin $I > 1/2$ in the sample. The related NSR rate $1/T_1$ is given by the general relation [2]

$$\frac{1}{T_1} = \langle\omega_Q^2\rangle\cdot\frac{\tau}{1+\omega^2\tau^2} \tag{2}$$

where ω is the effective Larmor frequency and $\langle\omega_Q^2\rangle$ denotes the mean-squared quadrupole interaction due to the fluctuating EFGs of the moving dislocations at the site of the probe nuclei, i.e. $\langle\omega_Q^2\rangle = \rho_m\cdot\omega_Q^2$ with ω_Q^2 being the mean-squared quadrupole interaction caused by a dislocation of unit length [3].

Applying appropriate low deformation rates $\dot{\varepsilon}$ and Larmor frequencies ω one can easily fulfill the condition $\omega\tau > 1$. Then, combining Eqs. (1) and (2) the dislocation-motion induced NSR rate $1/T_1|_D$ can be written as

$$\left.\frac{1}{T_1}\right|_D = \frac{\omega_Q^2}{\omega^2}\cdot\frac{1}{B\cdot x}\cdot\dot{\varepsilon} = C\cdot\frac{1}{x}\cdot\dot{\varepsilon} \tag{3}$$

One has to note here, that the exact calculation leads to the

* Corresponding author. Tel.: +231-755-3518; fax: +231-755-3516.
E-mail address: kanert@e3.physik.uni-dortmund.de (O. Kanert).

0038-1098/$ - see front matter © 2003 Elsevier Ltd. All rights reserved.
doi:10.1016/j.ssc.2003.12.018

same relation (3), except for a slightly modified prefactor C and a jump width dependence $g_Q(x)/x$ instead of $1/x$ with $g_Q(x) = 0$ for $x = 0$ and $g_Q(x) = 1$ for $x \geq 10^3 \cdot b$ [3]. Eq. (3) shows that a large NSR rate is expected for low effectice Larmor frequencies, i.e. one has to perform the NSR experiment in the rotating frame where ω is in the kHz range. Moreover, in order to observe the details of the dislocation dynamics during the short deformation time Δt (here about 100 ms) one has to detect the total time evolution of the nuclear magnetization $M_\rho(t)$ during Δt. We have developed a fast multi-window pulse sequence which measures the complete magnetization decay in the rotating frame, $M_\rho(t)$, in a single shot [4]. The sequence is triggered by the electronic control of the servo-hydraulic deformation device. Details of the setup are described elsewhere [5].

We have successfully applied the technique to study in-situ (i.e. during the deformation process) the dynamics of moving dislocations in ionic materials as well as in metals and dilute metallic alloys [6,7].

2. Experimental aspects and results

The experiments were performed on a series of NaCl single crystals of size $6 \times 6 \times 11$ mm^3 with varying Ca^{++} content ('ultrapure' ($<$0.1 ppm Ca^{++} and Mg^{++}), 4, 6.3, 10, 24 ppm) supplied by Dr Korth company, Kiel, Germany. The samples were plastically compressed along $\langle 100 \rangle$ slightly above room temperature (actual temperatures are given in the respective figures) at a constant strain rate $\dot{\varepsilon}$. The total deformation was within deformation stage I which is characterized by single slip of dislocations along $\langle 110 \rangle$ on primary (110) slip planes. During the deformation process the time evolution $M_\rho(t)$ of the ^{23}Na nuclear magnetization in the rotating frame was measured by means of the multi-window pulse sequence technique discussed in Section 1. The NMR experiments were performed in a cryomagnet with a magnetic field of 3.67 T while the effective locking field in the rotating frame was 0.27 mT corresponding to an effective Larmor frequency ω of the ^{23}Na probe nuclei of 2×10^4 s^{-1} in Eq. (3). For this, one has to consider also the contribution of the local field of the ^{23}Na spin ensemble [8]. Fig. 1 shows the normalized time evolution $M_\rho(t)/M_\rho(0)$ observed in ultrapure NaCl without ($\dot{\varepsilon} = 0$) and during deformation ($\dot{\varepsilon} = 0.44$ s^{-1}). The magnetization decay obeys an exponential law $M_\rho(t)/M_\rho(0) = \exp(-t/T_1)$ which points to a spatially homogeneous relaxation process with a uniform spin temperature. Moreover, the data demonstrate clearly the strong effect of the moving dislocations on the NSR rate $1/T_1$ rising from the background rate $1/T_1(\dot{\varepsilon} = 0) = 0.11$ s^{-1} to $1/T_1 = 1/T_1|_D + 1/T_1(\dot{\varepsilon} = 0) = 17$ s^{-1} at $\dot{\varepsilon} = 0.44$ s^{-1}, i.e. $1/T_1|_D \cong 1/T_1$ under the applied experimental conditions. By use of the data published in [9] one obtains a value of 127 μm for the coefficient C in Eq. (3) for ^{23}Na in NaCl under the applied experimental conditions. In

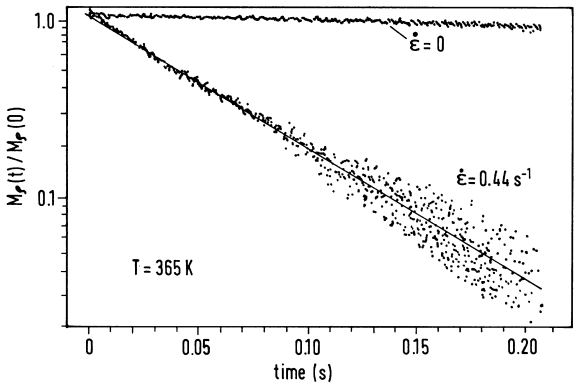

Fig. 1. Single-shot measurement of the ^{23}Na nuclear magnetization decay in the rotating frame, $M_\rho(t)$, in ultrapure single-crystalline NaCl without ($\dot{\varepsilon} = 0$) and during deformation ($\dot{\varepsilon} = 0.44$ s^{-1}). Deformation was along $\langle 100 \rangle$ at $T = 365$ K. The data were taken by a fast multi-window $T_{1\rho}$ sequence.

units of the Burgers vector $b = 3.98$ Å for NaCl the mean jump distance x/b can be calculated as $x/b = 3.2 \times 10^5 \cdot \dot{\varepsilon} \cdot T_{1D} = 8.3 \times 10^3$ in accord with other investigations [9].

Supposing that immobile forest dislocations build the major obstacles for the moving dislocations in ultrapure NaCl the related density $\rho_{Forest} \cong 1/x^2$ is about 10^7 cm^2 which is a typical number for pure alkali halides. However, as depicted in Fig. 2, in contrast to ultrapure NaCl the magnetization $M_\rho(t)$ in Ca^{++}-doped NaCl decays plainly non-exponentially under deformation. This is caused by a spatially inhomogeneous distribution of the Ca^{++} ions affecting the configuration of the forest dislocations. The Ca^{++} ions influence only indirectly the dislocation dynamics: The cross slip of screw dislocations is empeded by the interaction with Ca^{++}. With a reduced cross-slip less stable edge dislocation dipoles can be generated and as a consequence more separate slip bands have to be activated with increasing impurity content. Hence, the number of boundaries where the slip bands meet will increase. Optical measurements with polarized light on the deformed samples support the findings. The micrographs exhibit clearly the formation of separate slip bands in the Ca^{++} doped samples in contrast to analogous measurements in ultrapure NaCl. For instance, the separation of the slip bands in NaCl: 10 ppm Ca^{++} deformed to 2.6% was found to be about 0.2 mm.

As expected, a quenching procedure of the sample results in a more uniform distribution of the Ca^{++} related obstacles leading to a corresponding decrease of the curvature of the decay $M_\rho(t)$. This is demonstrated in Fig. 3, exhibiting the decays $M_\rho(t)$ in NaCl: 10 ppm Ca^{++} 'as grown' and after a quenching treatment (16 h at 500 °C, quenching to room temperature with about 20 °C/min) during deformation. Moreover, a slight enhancement of the deformation temperature does not change the curvature of $M_\rho(t)$. This is shown in Fig. 4 where the decays $M_\rho(t)$ are

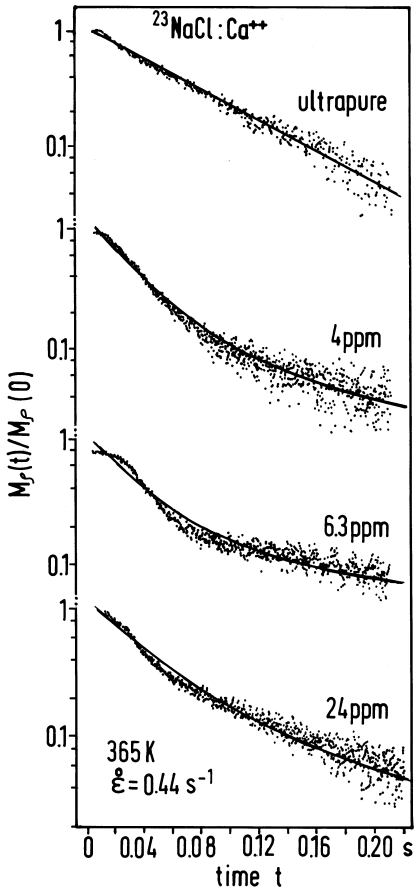

Fig. 2. Single-shot decays $M_\rho(t)$ of ^{23}Na observed during deformation ($\dot{\varepsilon} = 0.44\ s^{-1}$) in single-crystalline NaCl with different content of Ca^{++}. Solid curves are fits to the data by Eq. (8).

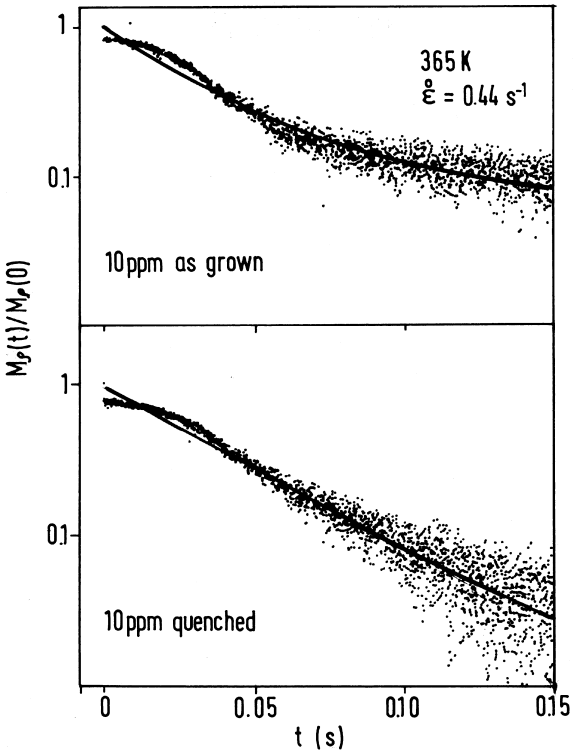

Fig. 3. Single-shot decays $M_\rho(t)$ of ^{23}Na in NaCl:10 ppm Ca^{++} 'as grown' and after quenching, respectively, measured at $\dot{\varepsilon} = 0.44 \times s^{-1}$. Solid curves are fits to the data by Eq. (8).

depicted for NaCl: 24 ppm Ca^{++} observed at 365 and 450 K without ($\dot{\varepsilon} = 0$) and during ($\dot{\varepsilon} = 0.44\ s^{-1}$) deformation. Of course, the background NSR rate $1/T_1(\dot{\varepsilon} = 0)$ increases with rising temperature according to $1/T_1(\dot{\varepsilon} = 0) \propto T^2$ due to phonon-assisted quadrupole fluctuations [2]. The shape of the decays under deformation, however, remains unchanged indicating that the non-uniform distribution of the Ca^{++}-related obstacles is unaffected by a slight increase of the deformation temperature.

3. Evaluation and discussion

As discussed in the last section the total magnetization $M_\rho(t)$ in Ca^{++}-doped NaCl relaxes heterogeneously, i.e. $M_\rho(t)$ can be expressed as a superposition of exponential decays with a site-dependent relaxation rate $\nu(x) = A/x$ where $A = C{\cdot}\dot{\varepsilon}$ (see Eq. (3)). Here, x denotes the local jump width of the moving dislocations which is controlled by the local density of the Ca^{++}-related obstacles. The total magnetization can be written as

$$M_\rho(t) = M_\rho(0) \int_0^\infty g(\nu)\, e^{-\nu t}\, d\nu \tag{4}$$

where $g(\nu)$ is the distribution function of the local relaxation rate ν which is proportional to the inverse of the local jump width x.

In order to obtain a simple analytical relation of $M_\rho(t)$ we suppose a box-like distribution for $g(\nu)$, i.e.

$$g(\nu) = \begin{cases} a = \text{const}, & \text{for } \nu_1 = A/x_1 \le \nu \le \nu_2 = A/x_2 \\ 0, & \text{otherwise} \end{cases} \tag{5}$$

where x_1 and x_2 denote the upper and lower limit, respectively, of the mean jump width x. The normalization condition $\int_0^\infty g(\nu)d\nu = 1$ yields $a = 1/(\nu_2 - \nu_1)$ for the parameter a in Eq. (5). Inserting Eq. (5) into Eq. (4) and performing the integration leads to an analytical expression for $M_\rho(t)$:

$$M_\rho(t) = \frac{M_\rho(0)}{(\nu_2 - \nu_1)t}[e^{-\nu_1 t} - e^{-\nu_2 t}] \tag{6}$$

As required, Eq. (6) exhibits the following limiting conditions:

$$\lim_{t\to 0} M_\rho(t) = M_\rho(0), \qquad \lim_{\nu_2 \to \nu_1 \equiv \nu} M_\rho(t) = M_\rho(0) e^{-\nu t}.$$

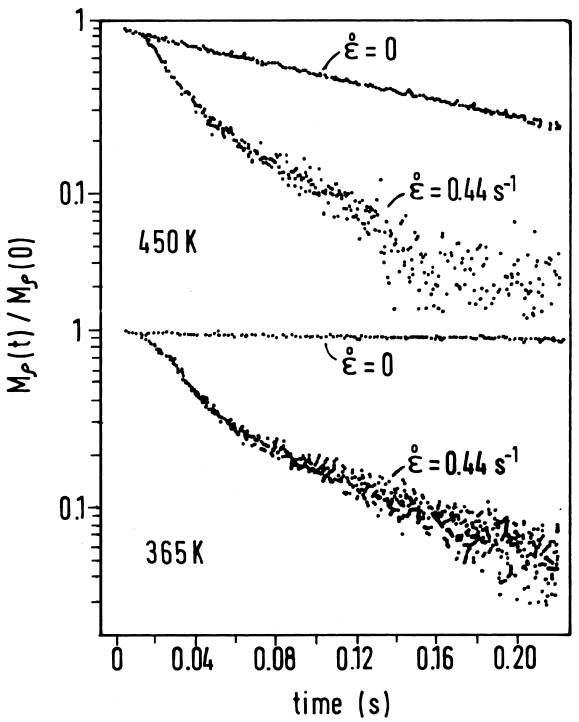

Fig. 4. Single-shot decays of ^{23}Na in NaCl: 24 ppm Ca^{++} observed at $\dot{\varepsilon} = 0$ and $\dot{\varepsilon} = 0.44\ s^{-1}$ for two different temperatures (365 and 450 K, respectively).

The second relation describes the expected mono-exponential decay of a uniform distribution of the mean jump width. Furthermore, the center of gravity $\langle\nu\rangle = \int_0^\infty \nu g(\nu)\,d\nu$ of the distribution function $g(\nu)$ is given by $\langle\nu\rangle = 1/2(\nu_1 + \nu_2)$.

Finally, it should be remarked that the distribution function $g(x)$ of the mean jump distance x is related to the function $g(\nu)$ by

$$g(x) = \begin{cases} \dfrac{1}{x^2}\dfrac{x_1 x_2}{x_1 - x_2,} & \text{for } x_2 \le x \le x_1 \\ 0, & \text{otherwise} \end{cases} \tag{7}$$

i.e. the constant distribution of $g(\nu)$ between ν_1 and ν_2 Eq. (5) corresponds to a $1/x^2$-dependence of $g(x)$ between x_2 and x_1.

The solid curves in Figs. 2 and 3 are fits to the data by use of Eq. (6) taking into account an additional small zero-point correction C, i.e.

$$M_\rho(t) = \frac{M_\rho(0)}{(\nu_2 - \nu_1)t}[e^{-\nu_1 t} - e^{-\nu_2 t}] + C \tag{8}$$

The corresponding best-fit parameters including the related centers of gravity $\langle\nu\rangle$ are listed in Table 1.

Obviously, the fitting procedure works well except for the deviations occuring at short times, i.e. at the onset of the deformation. The kind of deviation between the data and the fitting curves indicates that the servohydraulic deformation device does not start stepwise but gradually at $t = 0$, i.e. the deformation rate $\dot{\varepsilon}$ rises in a short time of about 40 ms from zero to the final value $\dot{\varepsilon} = 0.44\ s^{-1}$. Concerning the distribution function $g(\nu)$ (Eq. (5)) one should remark that other appropriate functions applied to Eq. (4) would probably fit the data, too. The width of the respective function, however, characterized by the lower and upper limits ν_1 and ν_2 (see Table 1) should be similar to that of the present function. Using again $C = 127\ \mu m$ for the coefficient in Eq. (3) the limits ν_1 and ν_2 can easily be rewritten to the corresponding limits $1/x_1$ and $1/x_2$ by $1/x = \nu/(C{\cdot}\dot{\varepsilon})$. Fig. 5 repesents these limits in units of the Burgers vector b as a function of the amount of Ca^{++} ions. The figure exhibits the following features:

Table 1
Summary of the parameters used for data fitting by Eq. (8) (solid curves in Figs. 2 and 3)

Ca^{++} content (ppm)	$\nu_1 = A/x_1$ (s^{-1})	$\nu_2 = A/x_2$ (s^{-1})	C	$\langle\nu\rangle$ (s^{-1})
0	17.0	17.0	0	17
4	10.0	60.0	0.015	35
6.3	6.0	60.0	0.035	33
10	8.0	58.5	0.039	33.25
24	8.6	40.2	0.015	24.4
10 (quenched)	15.0	40.0	0	27.5

The distribution $g(\nu)$ turns out to be not symmetric with respect to the value $b/x = 1.2 \times 10^{-4}$ of ultrapure NaCl but is shifted to larger values of b/x, i.e. to shorter mean jump distances. Surprisingly, the magnitude of the shift which is proportional to $\langle\nu\rangle$ listed in Table 1 varies only very weakly with rising Ca^{++} concentration. The findings are in sharp contradiction to the Friedel–Fleischer relation $b/x = \sqrt{C(Ca^{++})}$ which is based on the assumption of an equidistant distribution of Ca^{++}-vacancy dipoles in the

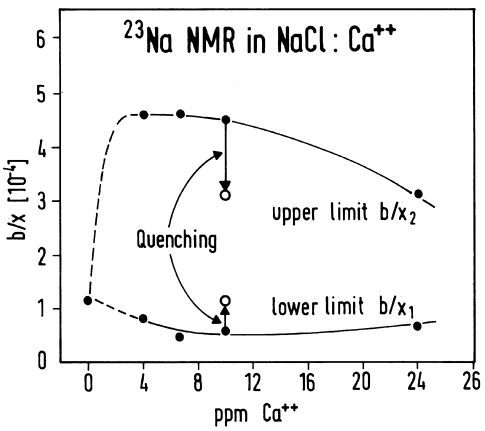

Fig. 5. Upper (b/x_2) and lower (b/x_1) limit of the distribution of the mean jump distance vs. Ca^{++} concentration as calculated from the corresponding values ν_1 and ν_2 listed in Table 1. Quenching leads to closer values for b/x_1 and b/x_2, i.e. to a more uniform distribution of the mean jump width x in the sample.

activated slip planes acting as obstacles for the mobile dislocations [10,11]. Depending on the respective Ca^{++} content the Friedel–Fleischer relation leads roughly to $b/x \approx 3 \times 10^{-3}$ which is about a factor of 20 larger than $\langle b/x \rangle \approx 1.5 \times 10^{-4}$ obtained from the values of $\langle \nu \rangle$ in Table 1. Hence, we propose that a remarkable fraction of the Ca^{++} ions form aggregates (dimers, trimers, etc.) which limits, however, the mean jump distance x only indirectly by variation of the dislocation configuration. The dislocation motion will take place more inhomogeneously in separate slip bands which becomes more closely spaced at increasing Ca^{++} concentration. As noted in Section 2 the formation of such separate slip bands is confirmed by optical measurements using polarized light. Moreover, the observed very small variation of $\langle \nu \rangle$ on the amount of Ca^{++} indicates that for a major part the dependence of the mean jump distance x on the impurity content is not directly caused by a change in mean distance between the impurities itself.

The width of the distribution $g(\nu)$ decreases slightly with rising Ca^{++} concentration, i.e. the resulting dislocation configuration becomes more uniform at elevated Ca^{++} content. This demonstrates again the indirect and complex effect of the impurity ions on the arrangement of the forest dislocations and the resulting dislocation dynamics.

As discussed in context with Fig. 3, a quenching procedure results in a distinct reduction of the width of the distribution $g(\nu)$ pointing to a nearly uniform distribution of the Ca^{++}-related obstacles. In particular, as shown in Table 1 the lower limit $\nu_1 = A/x_1$ of the distribution approaches the value ν of the ultrapure sample. It is interesting to note that in spite of the finite width of $g(\nu)$ for the quenched sample the corresponding magnetization $M_\rho(t)$ seems to decay mono-exponentially (solid curve in Fig. 3). However, small deviations from an exponential law become apparent only by an expansion of the measurements of $M_\rho(t)$ to sufficient large times.

Finally, we would like to remark that the present results summarized in Fig. 5 differ somewhat from those observed in earlier Ca^{++} doped NaCl [12]. However, in the first study both the Ca^{++} content and the applied temperature were considerably larger (7–690 ppm, and 150–300 °C, respectively) than those in the present study. At the elevated temperatures the Ca^{++} related defects start to perform localized motions. Moreover, the early results were obtained from a 'classical' $T_{1\rho}$-experiment, i.e. from just one data point of the magnetization decay $M_\rho(t)$, whereas in the present study the multi-window sequence measures the complete time evolution $M_\rho(t)$ including deviations from an exponential law. The improvement of the experimental method reduces distinctly uncertainties in the determination of the jump width x.

Acknowledgements

The work was financially supported by the Deutsche Forschungsgemeinschaft (DFG).

References

[1] E. Orowan, Z. Phys. 89 (1934) 634.
[2] D. Wolf, Spin Temperature and Nuclear-Spin Relaxation in Matter, Clarendon, Oxford, 1979.
[3] J.Th.M. De Hosson, O. Kanert, A.W. Sleeswyk, in: F.R.N. Nabarro (Ed.), Dislocation in Solids, vol. 6, North-Holland Pub. Co., Amsterdam, 1983, Chapter 32.
[4] K. Detemple, O. Kanert, J.Th.M. De Hosson, K.L. Murty, Phys. Rev. B 52 (1995) 125.
[5] H. Hackeloer, O. Kanert, H. Tamler, J.Th.M. De Hosson, Rev. Sci. Instrum. 54 (1983) 341.
[6] K.L. Murty, D. Begert, R. Münter, O. Kanert, Appl. Phys. Lett. 57 (1989) 628.
[7] J.Th.M. De Hosson, A. Huis in't Veld, H. Tamler, O. Kanert, Acta Metall. 32 (1984) 1205.
[8] K. Detemple, O. Kanert, K.L. Murty, J.Th.M. De Hosson, Phys. Rev. B 44 (1991) 1988.
[9] H. Neuhäuser, G. Schulz, Phys. Status Solidi (A) 45 (1978) 89.
[10] J. Friedel, Dislocations, Pergamon, Oxford, 1964.
[11] R. Fleischer, Acta Metall. 10 (1962) 835.
[12] W.H.M. Alsem, J.Th.M. De Hosson, R. Muenter, H. Tamler, O. Kanert, Philos. Mag. A 46 (1982) 469.